Food Chemistry: X 3 (2019) 100029

Contents lists available at ScienceDirect

Food Chemistry: X

journal homepage: www.journals.elsevier.com/food-chemistry-x

Alterations in physicochemical and functional properties of buckwheat straw insoluble dietary fiber by alkaline hydrogen peroxide treatment

Xuemei Meng, Fang Liu, Yao Xiao, Junwei Cao, Min Wang*, Xuchang Duan*

College of Food Science and Engineering, Northwest A&F University, 712100 Yangling, PR China

ARTICLE INFO

Keywords:
Alkaline hydrogen peroxide
Insoluble dietary fiber
Buckwheat
Functional properties
Mechanism

ABSTRACT

To enhance the physicochemical and functional properties of insoluble dietary fiber (IDF) from buckwheat straw, we investigated the effects of alkaline hydrogen peroxide (AHP) treatment. Electron microscopy showed that the IDF had regular and compact tubes that turned into wrinkled lamellar products. After AHP treatment, X-ray diffraction indicated that the crystalline structure of the IDF was perturbed. And an undesirable decrease was observed in the content of hydroxybenzoic acid derivatives, hydroxycinnamic acid derivatives, flavonoids and the antioxidant capacity of IDF modified by AHP; however, the hydration properties (such as water holding capacity), α-amylase inhibition activity and glucose adsorption capacity of IDF were significantly enhanced by AHP. Furthermore, AHP led to a redistribution of monosaccharides in soluble dietary fiber and IDF, an interesting finding hinting at the mechanism and potential applications of AHP modification of IDF. In this study, AHP enhanced the physiological and functional properties of buckwheat straw IDF.

1. Introduction

Buckwheat (*Fagopyrum esculentum*) is one of the most important functional foods and traditional medicines worldwide. It is a good source of starch, protein, lipid, dietary fiber (DF) and minerals together with other beneficial health components (Yu, Chen et al., 2018). In 2016, buckwheat cultivation accounted for 2.3 million hectares, and global production was almost 2.3 million tons (Kalinová, Vrchotová, & Tříska, 2018). Buckwheat groats are widely used in commercial products, such as alcoholic beverages, blended breads, and noodles, owing to their functional and organoleptic properties (Yu, Chen et al., 2018). Buckwheat straw, an important part of buckwheat, is used to feed livestock or is incinerated in situ. Owing to its richness in cellulose and hemicelluloses, buckwheat straw is considered a potential source of insoluble DF (IDF) that may be used to improve the conversion rate and economic benefits of buckwheat cultivation.

DF is defined as carbohydrate polymers with ten or more monomeric units that are not hydrolyzed by the endogenous enzymes in the small intestine in humans (Codex Alimentarius, 2017). DF is a complex component divided into IDF and soluble DF (SDF) according to solubility in water (Li, Feng, Niu, & Yu, 2018). Most of the DF from plant sources is classified as IDF, which contains functional groups such as phenolics, carboxylic acids, aldehydes, ketones and ether linkages (Zheng & Li, 2018). Cellulose, hemicelluloses and lignin are the main components of IDF, which has the physiological functions of supporting the growth of intestinal flora, increasing the volume of feces, decreasing the intestinal transit and inhibiting pancreatic lipase activity (Yu, Bei, Zhao, Li, & Cheng, 2018). In buckwheat straw, the high content of cellulose, hemicelluloses and lignin is the major contributor to the plant's ability to survive in harsh Alpine highlands. Buckwheat straw is considered a potential and abundant source of IDF.

Hydrogen peroxide, an efficient low toxicity and low-cost fungicide, is widely used in industrial bleaching, surgical disinfection and other fields. Alkaline hydrogen peroxide (AHP) has been used to pretreat lignocellulosic biomass to decrease its resistance to enzymatic hydrolysis and improve its bioavailability (Lewis, Montgomery, Garleb, Berger, & Fahey, 1988). This treatment plays an important role in cellulose degradation, hemicellulose solubilization and lignin removal (Dutra et al., 2018). The reaction products of AHP treatment of biological materials are oxygen and water, and there is no secondary pollution. Many studies have shown that AHP treatment significantly improves the content and functional properties of SDF (Li et al., 2018). However, the effects of AHP treatment on the structural and functional properties of IDF have scarcely been reported.

In this study, we examined AHP treatment, which plays an important role in degradation of lignin-carbohydrate complexes. The aim of this study was to explore the effect of AHP treatment on the composition, structure and various functional properties of buckwheat

* Correspondence author.
E-mail addresses: wangmin20050606@163.com (M. Wang), duanxc1965@163.com (X. Duan).

https://doi.org/10.1016/j.fochx.2019.100029
Received 14 September 2018; Received in revised form 9 April 2019; Accepted 7 May 2019
Available online 14 May 2019
2590-1575/ © 2019 The Authors. Published by Elsevier Ltd. This is an open access article under the CC BY-NC-ND license (http://creativecommons.org/licenses/BY-NC-ND/4.0/).

straw IDF and to explain the mechanism of action.

2. Materials and methods

2.1. Materials

Buckwheat straw (Xi Nong 9940) was purchased in Yu Lin, Shannxi, China. Buckwheat straw flour was obtained by washing, air-drying, smashing and sieving (40 mesh sieve). The flour was stored at −20 °C until use.

Heat-stable α -amylase and protease solutions were purchased from Megazyme. The wheat-IDF named Unicell WF 90 was produced by Interfiber Company (Warsaw, Poland). Standard monosaccharides (l-rhamnose, d-arabinose, l-fucose, d-xylose, d-mannose, d-glucose, and d-galactose) and 2,2-diphenyl-1-picrylhydrazyl (DPPH) were purchased from Sigma–Aldrich (St. Louis, USA). A glucose determination kit was purchased from Jiancheng Technology Company (Nanjing, China). All other chemicals used in this study were of analytical grade.

2.2. Preparation of insoluble dietary fiber from buckwheat straw

Buckwheat straw was first treated with AHP. Buckwheat straw powder was mixed with hydrogen peroxide solution (17%; pH 11.0) at a ratio of 1:18 and stirred for 30 min. After being washed with distilled water, the solid powder was air-dried at 40 °C.

The IDF was extracted through a complex enzyme method. The untreated buckwheat straw power and treated buckwheat straw power were boiled in distilled water for 2 h, and 1% α -amylase (20000 U/g) solution was added to the suspension in a water bath above 95 °C and incubated for 35 min. Then, 0.5 g of protease (100 U/mg) was added at pH 9–11 and 45 °C with constant shaking for 30 min. The solid matter was then filtered with water-washing. Finally, the solid matter was air-dried at 40 °C overnight to obtain original buckwheat straw IDF (O-IDF) and modified buckwheat straw IDF (M-IDF).

2.3. Scanning electron microscopy

The surface and microstructure of IDF were observed through scanning electron microscopy (SEM; JSM-6360LV Scanning Electron Microscope, Akishima, Tokyo, Japan) at 20 kV. Powder samples were mounted on metal stubs and sputter-coated with a 10-nm gold and palladium layer through ion sputtering. Representative micrographs were taken for each sample at 1500× and 6000× magnification.

2.4. Crystalline structure

X-ray diffraction (XRD) analysis of the dried sample was carried out according to (Ullah et al., 2018) with slight changes. The XRD pattern was obtained from a D8 ADVANCE A25 Diffractometer (Bruker, Karlsruhe, Bundesrepublik Germany) by using Cu Kα radiation (λ = 0.1541 nm) Å within the scanning range of 5–80°, with coupling with a scanning speed of 2° (2θ) min^{-1}.

2.5. Color analysis

Color values of IDF were measured with a Ci7600 colorimeter (X-rite, Grand Rapids, Michigan, USA). The color values were expressed by using Commission Internationale de L'Eclairage (CIE) Lab* coordinates, where L* represents the luminosity (0 = black; 100 = white), a* the redness (a* > 0) or greenness (a* < 0), and b* the blueness (b* > 0) or yellowness (b* < 0). The whiteness index (WI) was then determined with the following equation (Ullah et al., 2018):

$$WI = 100 - \sqrt{(100-L)^2 + a^2 + b^2}$$

2.6. Gas chromatography analysis

Hydrolysis and derivatization of IDF were performed according to a previous study (Wang et al., 2017). The sample solutions were filtered through an 0.45 mm filter membrane before determination. Gas chromatography was used to analyze the monosaccharide composition of the IDF samples. The GC-2014C gas chromatography (Shimadzu, Japan) system was equipped with a flame ionization detector (FID) (medium polar capillary column DB-17, 0.25 mm × 30 m × 0.25 μm). Nitrogen was used as the carrier gas with a constant flow rate of 1.5 mL/min. The flow rates of air and hydrogen were 450 mL/min and 60 mL/min, respectively. The injection volume was 1 μL, and the detection temperature was 280 °C. The temperature programming was as follows: the initial temperature of 180 °C was held for 2 min, increased to 210 °C with a linear gradient in 5 min, held for 2 min, increased to 215 °C at 0.3 °C/min and held for 20 min, and finally increased to 240 °C at 6 °C/min and held for 10 min. Standard monosaccharides including glucose, mannose, galactose, rhamnose, arabinose and xylose were used to calculate the content of monosaccharide composition.

2.7. Phenolic profiles and content of IDF

The analysis of phenolic compounds was performed with high performance liquid chromatography (HPLC), according to (Webber et al., 2014) with slight modification. Briefly, 1 g of IDF was mixed with 80% acetone solution under stirring for 10 min at 0 °C. Following centrifugation the supernatant was evaporated at 45 °C, a procedure that was repeated twice, and dissolved in 10 mL methanol. All samples were analyzed with an LC-20A HPLC system (Shimadzu, Japan) equipped with an ultraviolet detector and a chromatographic column. The conditions used were as follows: column temperature 30 °C; injection volume 20 μL; detection wavelength 320 nm/280 nm; flow rate 0.8 mL/min; total HPLC run time 55 min; and mobile phase, 2% acetic acid in deionized water (solution A) and methanol (solution B). The mobile phase was programmed as follows: 0–10 min, 5%–30% B; 10–35 min, 30%–50% B; 35–40 min, 50%–60% B; 40–45 min, 60%–70% B; 45–50 min, 70%–5% B; 50–55 min, 5% B. For the analysis, all samples were filtered through a 0.45 μm membrane filter. The samples were identified by comparing the retention times with known authentic standards.

2.8. Hydration properties of buckwheat straw IDF

The water holding capacity (WHC), water retention capacity (WRC), oil retention capacity (ORC) and water swelling capacity (WSC) were determined according to reported methods with slight modifications.

The samples (0.5 g) were weighed in a 10 mL centrifuge tube. After being mixed with 5 mL distilled water, the samples were placed for 1 h at 37 °C, and then the water was filtered out. The WHC values of the samples were calculated as:

$$WHC = \frac{W_3 - W_2}{W_1}$$

where W_1 is the weight of the sample (0.5 g), W_2 is the total weight of the sample and centrifuge tube before filtering (g), and W_3 is the total weight of sample and centrifuge tube after filtering (g).

The 0.5 g sample was weighed in a 10 mL centrifuge tube and hydrated in 5 mL distilled water for 1 h at 37 °C, then centrifuged at 4472 × *g* for 10 min. The excess water was removed by inversion. The weight of the resulting residue was recorded. WRC was calculated with the following equation:

$$WRC = \frac{W_3 - W_2}{W_1}$$

where W_1 is the weight of the sample (0.5 g), W_2 is the total weight of the sample and centrifuge tube before centrifugation (g), and W_3 is the

total weight of the sample and centrifuge tube after centrifugation (g).

The sample (0.5 g) was mixed with soybean oil in a centrifuge tube and incubated for 1 h at 37 °C. The mixture was then centrifuged at 4472 × *g* for 10 min. The centrifuge tube was inverted to remove excess soybean oil. ORC was expressed as follows:

$$\text{ORC} = \frac{W_3 - W_2}{W_1}$$

where W_1 is the weight of the sample (0.5 g), W_2 is the total weight of the sample and centrifuge tube before centrifugation (g), and W_3 is the total weight of the sample and centrifuge tube after centrifugation (g).

The volume of each 0.5 g sample was recorded in a 10 mL centrifuge tube with 5 mL distilled water. After mixing to uniformity, the mixture was incubated for 24 h at 37 °C. The volume of the sample after expansion was recorded. WSC was calculated with the following equation:

$$\text{WSE} = \frac{V_2 - V_2}{W}$$

where V_1 is the volume of DF before hydration (mL), V_2 is the volume of the hydrated DF (mL), and W is the weight of DF before hydration (g).

2.9. Measurement of in vitro antioxidant activity of IDF

2.9.1. DPPH radical scavenging capacity

The ability of extracts to scavenge the DPPH radical was analyzed with the colorimetric method described by (Yan, Ye, & Chen, 2015) with slight modification. Briefly, 20 mg of IDF was mixed with 2 mL of 6×10^{-5} M DPPH prepared in ethanol solution. The absorbance was determined at 517 nm after 25 min in darkness.

2.9.2. Ferric ion reducing antioxidant power assay

Ferric ion reducing antioxidant power (FRAP) assays were conducted on the basis of published research (Nieto Calvache, Cueto, Farroni, de Escalada Pla, & Gerschenson, 2016). In brief, Fe^{3+} pyridine-triazine can be reduced to Fe^{2+}. IDF samples were mixed with 3 mL FRAP solution and incubated for 5 min at 37 °C, then centrifuged at 4672 × *g* for 5 min; the supernatant was measured at 593 nm to determine the absorbance of the samples. A standard curve was prepared with different concentrations (0.2–0.8 mM) of $FeSO_4$.

2.9.3. Hydroxyl radical scavenging activity

The method reported by Raghavendra et al. (2006) was used with some modifications. Ten milligrams of the SDF sample was diluted to 2 mL with PBS buffer solution (0.1 mol/L, pH 7.4); then 1.0 mL of phenanthroline solution (0.75 mo1/L), 1 mL $FeSO_4$ solution (6 mmol/L) and 1 mL hydrogen peroxide (8 mmol/L) were added. The samples were incubated for 60 min at 37 °C, and a 3900H spectrophotometer (Hitachi Limited, Tokyo, Japan) was used to measure absorption at a wavelength of 536 nm.

2.9.4. Superoxide anion radical scavenging activity

The scavenging rate of the superoxide anion ($\cdot O^{2-}$) was measured with the pyrogallol autoxidation method. Four milliliters of Tris-HCl buffer solution (0.05 mol/L, pH 8.2) was placed in a water bath at 25 °C to preheat and then completely mixed with 10 mg IDF, 1 mL pyrogallol (25 mmoL/L) and 1 mL distilled water. The mixture was incubated in a water bath for 5 min at 25 °C. HCl (100 μL of 8% solution) was used to terminate the reaction, and the absorbance of the mixture was measured with a 3900H spectrophotometer (Hitachi Limited, Tokyo, Japan) at 320 nm. Tris-HCl buffer was used as reference solution.

The formula used to calculate superoxide anion radical scavenging activity was as follows:

$$\text{Scavenging rate} = \left(1 - \frac{A_1 - A_2}{A_3}\right) \times 100\%$$

where A_1 is the absorbance of samples, A_2 is the absorbance of samples and 3 mL distilled water, and A_3 is the absorbance of Tris-HCl buffer, 1 mL distilled water and 1 mL pyrogallol.

2.10. α -amylase inhibitory activity inhibition ratio

Analysis of the α-amylase inhibitory activity of IDF samples was performed according to the method described by Xie, Wang, Wu, and Wang (2017). A 0.1 g sample was mixed with 25 mL of potato starch (4 g/100 mL, pH 6.5) and 0.1 g of α-amylase at 37 °C in a shaking water bath for 2 h. The solution was centrifuged at 2862 × *g* for 5 min. The glucose content of the supernatant was determined with a glucose assay kit.

2.11. Glucose adsorption capacity

The glucose adsorption activity of the IDF was investigated in 0.5 g of sample in 50 mL glucose solution with glucose concentrations of 10, 50, 100 and 200 mmol/L. After continuous stirring at 37 °C for 2 h, the solution was centrifuged at 2862 × *g* for 5 min. The supernatant was collected, and the final glucose concentration was determined with a glucose assay kit (Jiancheng Technology, Nanjing, P.R. China).

2.12. Statistical analysis

Each test was carried out in triplicate. Analytical values of experiments are shown as mean ± standard deviation. Statistical analyses were performed with one-way analysis of variance (ANOVA). $P < 0.05$ was considered statistically significant. Duncan tests were performed in SPSS, version 18.0 (SPSS, Chicago, Illinois, USA).

3. Results and discussion

3.1. SEM

The SEM micrographs (Fig. 1) of IDF before and after modification were magnified 1500× and 6000×. As shown in Fig. 1a, O-IDF had a tubular shape with a compact and integrated texture, which might have been from the vascular tissue of the buckwheat straw, which has roles in transport and supporting the plant. A smooth surface with a small amount of starch granules is visible in Fig. 1a′, thus indicating that the structure of buckwheat straw was not destroyed by α -amylase and protease during the extraction of IDF. Cellulose, hemicelluloses, lignin, protein and ash were present in different proportions in buckwheat straw; these components play specific roles in sustaining life and interacting in a complex matrix called the lignucellulosic biomass. The recalcitrance of the biomass toward enzymatic attack not only decreases the functional characteristics of IDF but also hinders its transformation into valuable products. A previous study has reported that the AHP pretreatment method decreases biomass recalcitrance and facilitates hemicellulose degradation and delignification (Carlos, 2016). Fig. 1b, b′ shows the microstructure structure of the IDF after AHP treatment. After some structural breakdown and transformation, M-SDF showed a wrinkled surface, owing to the disintegration of lignocellulose. Hemicelluloses, which serve as ligaments in lignocelluloses, were seen as highly branched polymers with negligible crystallinity and a low degree of polymerization, thus making the structure easy to disrupt with perhydroxyl anions, the key reactive species created according to Eq. (3) during AHP pretreatment. $H_2O_2 + \underset{pH = 11.6}{\longleftrightarrow} \Leftrightarrow H_2O + HOO^-$(3) (Dutra et al., 2018). Because of the recalcitrance, cellulose was retained as the main framework of M-IDF. Alkaline treatment of lignocellulose swelled the biomass substrate, thus resulting in increases in WHC, ORC and expansion (Carlos, 2016)

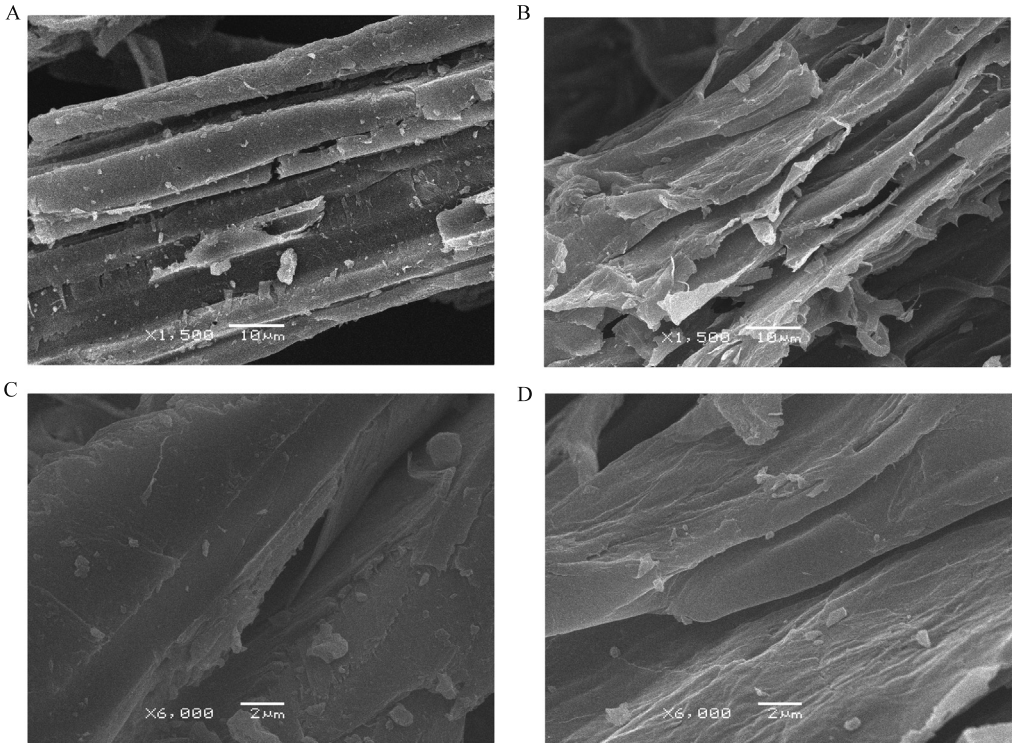

Fig. 1. Scanning electron microscopy (SEM) of insoluble dietary fiber obtained from buckwheat straw before and after alkaline hydrogen peroxide treatment. a and a′ represent the original buckwheat straw insoluble dietary fiber (O-IDF) at low and high magnification, respectively; b and b′ represent the modified buckwheat straw insoluble dietary fiber by alkaline hydrogen peroxide (M-IDF) at low and high magnification, respectively.

3.2. Crystalline structure of IDF

The crystalline structure of the IDF was analyzed with XRD, and the diffractograms are plotted in Fig. 2. Both O-IDF and M-IDF exhibited prominent crystalline peaks in the (0 0 2) diffraction direction at 22.34° and 15.90°, the typical cellulose I type diffraction angles, and one noncrystalline peak at 34.70° (Sheltami, Abdullah, Ahmad, Dufresne, & Kargarzadeh, 2012). The peak positions were not changed in M-IDF and O-IDF, thus indicating that AHP treatment did not alter the crystal type of IDF. The diffraction peak of M-IDF at 2θ of 15.70° was more irregular than that of O-IDF, possibly because of denaturation of cellulose during AHP treatment (Ma & Mu, 2016). The intensity of the diffracted peaks (22.34°) was enhanced in M-IDF as compared with O-IDF. In addition, the degree of crystallinity of M-IDF (37.98%) was significantly ($p < 0.05$) higher than that of O-IDF (22.34%), probably because of degradation of amorphous hemicelluloses (Rehman et al., 2014).

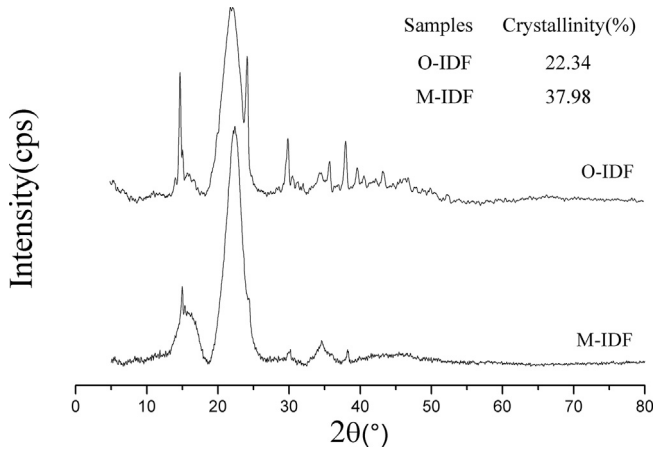

Fig. 2. Crystalline structure of IDF before and after alkaline hydrogen peroxide treatment. 2θ, diffraction angle; O-IDF, original buckwheat straw insoluble dietary fiber; M-IDF, modified buckwheat straw insoluble dietary fiber treated with alkaline hydrogen peroxide.

According to the literature, the crystalline region of IDF is mostly derived from the presence of cellulose, whereas non-crystalline cellulose, hemicelluloses and lignin are the main contributors to the amorphous region (Ma & Mu, 2016). During AHP treatment, the links among cellulose microfibers and hemicelluloses, hemicelluloses and lignin might be broken, thus leading to higher lignin and hemicellulose solubilization in the liquid fraction. The increased crystallinity of M-IDF mainly results from the removal of starch and lignin, and the hydrolysis of hemicelluloses and the amorphous portion in cellulose (Wen, Niu, Zhang, Zhao, & Xiong, 2017). The results were also in accordance with the changes observed through SEM (shown in Fig. 1).

3.3. Color analysis

The color of food ingredients is an important quality parameter affecting the potential application of IDF in the food industry and other industries (Ullah et al., 2018). CIE values (L*, a* & b*) along with the WI, chromas and hue angle of the IDF before and after AHP treatment are presented in Table 1. The lightness of M-IDF (89.88) was significantly ($p < 0.05$) higher than that of O-IDF (61.93), and the value of a* (redness) was significantly lower than that of O-IDF ($p < 0.05$), which was 5.07 to 0.13. The buckwheat straw IDF, which was prone to redness, might contain more anthocyanins and may be applied in meat products such as beef burgers and sausages, and fruit products such as strawberry jam (Diedericks & Jideani, 2015). However, the b* (yellowness) (representing blueness or yellowness) value was not significantly different between the two samples. The value of whiteness significantly increased, and the chromas decreased, after AHP treatment, thus suggesting destruction of the chromogenic substance in the buckwheat straw. The chlorophyll, carotenoid and flavonoid (including anthocyanin) compounds, whose structures contain chromophoric groups (i.e., C=C, C=O and C=N), can make buckwheat straw bright and colorful. There are two necessary reactive species for AHP treatment: H_2O_2 and alkalinity H_2O_2, a bleaching agent, can destroy or modify chromophore structures in the substrate. The alkaline conditions can cause H_2O_2 decomposition, thereby producing pre-hydroxyl radicals (HOO·), which attack the chromophore and bleach the

Table 1
CIE values (L*, a* & b*) whiteness index, chroma and hue angle of the IDF before and after alkaline hydrogen peroxide treatment.

Sample	L*	a*	b*	WI	C	H
O-IDF	61.93 ± 0.06^{b}	5.07 ± 0.01^{a}	11.41 ± 0.2	59.94 ± 0.11^{b}	12.45 ± 0.18^{a}	66.02 ± 0.38^{b}
M-IDF	89.88 ± 0.11^{a}	0.13 ± 0.11^{b}	11.3 ± 0.04	84.83 ± 0.04^{a}	11.3 ± 0.03^{b}	89.31 ± 0.55^{a}

L*, lightness; a*, red, (+a*) to green (−a*) range; b*, yellow (+b*) to blue (−b*) range; WI, whiteness index; C, chroma; H, hue angle; O-IDF, original buckwheat straw insoluble dietary fiber; M-IDF, modified buckwheat straw insoluble dietary fiber by alkaline hydrogen peroxide; AHP, alkaline hydrogen peroxide. Results were expressed as the means ± standard error of the triplicate measurements. Means with different lowercase letters superscripts in the same column are significantly different at $p < 0.05$. NS indicates that values in the same column are not significantly different.

substrate. A synergistic effect between H_2O_2 and alkalinity (reaction pH) is necessary for the efficient AHP pretreatment of biomass (Dutra et al., 2018; Lewis et al., 1988).

In addition, lignin, a polymer composed of three basic phenylpropanol units, can be defined as a non-crystalline polyphenol material; it is also regarded as a chromogenic substance in buckwheat stalks. Bleaching of IDF during AHP treatment was also a consequence of the reduction of lignin chromophore structures, as also confirmed by the decrease in antioxidation (Fig. 3b). The chroma of M-IDF was lower than that of O-IDF, probably because of the reducibility of flavonoids, especially anthocyanin, in accordance with the decrease in the polyphenol content (Table 3). Furthermore, the AHP treatment also increased the hue angle of IDF.

3.4. Gas chromatography analysis

Table 2 shows the sugar composition (relative molar percent) of the IDF isolated from buckwheat straw. Both IDF samples contained rhamnose, arabinose, xylose, glucose and galactose. In terms of peak area, xylose (71.27%) was the major monosaccharide of O-IDF and was followed by glucose (13.69%). The main constituent of M-IDF was glucose 68.41%), which was followed by rhamnose (10.15%). The high content of xylose in O-IDF might be related to hemicelluloses. The enzymes α -amylase and protease did not effectively decompose the lignocellulose biomass. A large amount of hemicellulose was retained in O-IDF. Xylan, which is made of xylose units linked by β-(1,4) glycosidic bonds, might be the major hemicellulose in O-INF. Except for xylan, some araboxylan probably existed in the IDF. The decrease in xylose content and the increase in glucose after AHP treatment were probably attributable to the dissolution of hemicelluloses and the increase in cellulose ratio in M-IDF, as demonstrated by the change in xylose content in SDF. The strong hydrogen bonds in cellulose chains makes cellulose stable to enzymatic or chemical attack (Dutra et al., 2018; Sangnark & Noomhorm, 2004). In addition, arabinose and rhamnose were detected in M-IDF and showed a higher ratio than that O-IDF. The different proportions of these sugars between O-IDF and M-IDF might be attributable to the formation of a gel. The gel formed after AHP treatment could not be separated from the IDF by filtering the enzymatic hydrolysate and thus remained in the M-IDF.

3.5. Phenolic profiles and content of IDF

The derivatives of hydroxybenzoic acid, hydroxycinnamic acids and flavonols of untreated and AHP-treated samples are presented in Table 3. Thirteen phenolics were detected in the O-IDF, including gallic acid, protocatechuic acid, syringic acid, p-hydroxybenzoic acid, tannic acid, caffeic acid, cinnamic acid, ferulic acid, chlorogenic acid, rutin, quercetin, and kaempferol. Ten phenolics were found in the M-IDF, although only trace amounts of ellagic acid and kaempferol were detected. *p*-coumaric acid was the most predominant monomeric phenol among the phenolics in the IDF, accounting for more than 47.6% of the total monomeric phenols, followed by ferulic acid and protocatechuic acid. In contrast, gallic acid was the most abundant among the phenolics in M-IDF, accounting for 49.8% of the total monomeric phenolics. Hydroxybenzoic acids derivatives, such as protocatechuic acid, were components of complex structures such as lignin, whereas the hydroxycinnamic acid derivatives such as ferulic acid were mainly bound to structural components of the cell wall (cellulose, lignin and protein) through ester linkages. The concentrations of derivatives of hydroxybenzoic acid of M-IDF were significantly lower than those in untreated IDF, thus suggesting the release of polyphenols from their strong associations with macromolecules in the food matrix after AHP treatment. Several peroxide derived reactive species are generated from H_2O_2 under alkaline conditions, one of which is the perhydroxyl anion (–). In alkaline medium, the hydroperoxide anion can react with H_2O_2, thus leading to the formation of hydroxyl radicals (HO·) and superoxide anion radicals ($O^{2-}\cdot$). All these compounds are responsible for the depolymerization effect on hemicellulose, lignin and cellulose fractions. Lignin is probably the most important site for chemical attack by radicals (Dutra et al., 2018). Hydroxybenzoic acid derivatives such as protocatechuic acid would also be attacked by radicals. M-IDF had substantially lower amounts of caffeic acid, coumaric acid, ferulic acid, cinnamic acid, chlorogenic acid and hydroxyl cinnamic acid—all of which are hydroxyl cinnamic acid derivatives (57 mg/g)—than O-IDF (1300 mg/g). In general, much lower concentrations of phenolics were present after treatment with AHP (Lewis et al., 1988). Approximately 95% of grain phenolic compounds are covalently linked to cell wall polysaccharides through ester bonds. The predominant mechanism for linking cell wall polysaccharides is the formation of several different diferulates via radical coupling reactions such as 5,5-diferulic acid. The presence of ferulic acid not only serves as a bridge structure between chains of polysaccharides but also plays a major role in cross-linking polysaccharides to lignin (Sanz-Pintos et al., 2017; Vitaglione, Napolitano, & Fogliano, 2008). Remarkably, coumaric acid and ferulic acid decreased by 100 times and 77 times, respectively (Table 3). O-IDF had higher concentrations of all measured phenolic compounds except gallic acid, and the compounds derived from hydroxycinnamic acid were more abundant than those derived from hydroxybenzoic acids, in accordance with the description of Vitaglione et al. (2008). In addition, the O-IDF contained markedly more detectable flavonoids, including rutin, quercetin and kaempferol, than the M-IDF. In summary, the total content of phenolics in O-IDF was nearly 9.5 times that in treated samples (from 1716.21 mg/g to 181.46 mg/g), and similar results have been found in wheat straw (Lewis et al., 1988). This discrepancy might be mainly attributable to depolymerization of fibrous matrixes by AHP treatment. Whether the IDF phenolic compound fraction can exert any antioxidant action itself, without any chemical hydrolysis, is unclear (Vitaglione et al., 2008). Some structural breakdown and transformation are seen in M-IDF, and the phytochemicals embedded in the fibrous matrix, including phenolics, are easily released (Zhang, Wang, Qu, Wei,

Table 2
Monosaccharide composition of the IDF before and after alkaline hydrogen peroxide treatment.

Percentage (%)	rhamnose	arabinose	glucose	galactose
O-IDF	5.29	3.20	13.69	6.56
M-IDF	10.15	8.30	68.41	6.85

Table 3
Phenolic profiles and content of IDF samples before and after modified.

		Name (mg/kg)	O-IDF	M-IDF
phenolic acids	derivatives of hydroxy benzoic acid	gallic acid	41.19 ± 2.12^{b}	94.32 ± 5.53^{a}
		protocatechuic acid	200.10 ± 37.81^{a}	5.76 ± 0.13^{b}
		syringic acid	28.56 ± 1.48^{a}	2.47 ± 0.02^{b}
		p-hydroxybenzoic acid	17.48 ± 3.15^{a}	4.74 ± 0.70^{b}
		ellagic acid	7.43 ± 0.68	–
	derivatives of hydroxyl cinnamic acid	caffeic acid	10.86 ± 1.83^{a}	2.02 ± 0.32^{b}
		p-coumaric acid	817.59 ± 40.74^{a}	8.81 ± 0.42^{b}
		cinnamic acid	42.04 ± 1.02^{a}	30.46 ± 5.00^{b}
		ferulic acid	385.99 ± 32.58^{a}	4.99 ± 1.52^{b}
		chlorogenic acid	43.02 ± 2.18^{a}	10.61 ± 1.29^{b}
flavonoids		rutin	29.17 ± 4.50^{a}	1.18 ± 0.32^{b}
		quercetin	30.10 ± 6.94^{a}	16.10 ± 3.42^{b}
		kaempferol	63.16 ± 1.01	–

Data were expressed by means ± SD (n = 3). Values in the same row with different lowercase letters are significantly different ($p < 0.05$). O-IDF, original buckwheat straw insoluble dietary fiber; M-IDF, modified buckwheat straw insoluble dietary fiber by alkaline hydrogen peroxide. –, undetected.

& Li, 2018). Lignin encrustation of cell wall polysaccharides had been proposed as a mechanism by which lignin limits the degradation of cell wall carbohydrates. AHP would disrupt the three-dimensional lignin structure encrusting the cell wall carbohydrates. The removal of total lignin or the alteration of lignin composition in the three dimensional structure as a result of AHP treatment may be attributed to a reduction of phenolic compounds (Sangnark & Noomhorm, 2004). Nevertheless, the results under this condition corresponded not to the direct release of small phenolic compounds from the food matrix but instead to the partial degradation of phenolics. We cannot rule out the possibility that AHP treatment may degrade some of the original phenolic structures. Consequently, the depolymerization of buckwheat straw biomass by AHP strongly influences the IDF structure and physical properties, thus further validating the antioxidant capacity and SEM results.

3.6. Hydration properties of IDF

The WHC, WRC, WSC and ORC of each IDF sample before and after AHP treatment were measured and are summarized in Fig. 3(a).

The WHC is the quantity of water that remains bound to the hydrated fiber without the application of an external force (pressure or centrifugation), according to research by Raghavendra et al. (2006); it is affected by the composition, molecular structure, particle size, surface area and porosity of the DF (Ullah et al., 2018). WHC is an important property of DF in both physiological and technological aspects. Fig. 3(a) shows that the WHC of O-IDF and M-IDF was 7.10 g/g and 16.15 g/g, respectively. Both O-IDF and M-IDF also exhibited higher WHC values than the wheat IDF reference ($p < 0.05$) and agricultural by-products from other fibers, e.g., 2.58 g/g from tartary buckwheat bran fiber (Zhou, Qian, Zhou, & Zhang, 2011), 3.6 g/g from rice bran DF (Wen et al., 2017), 6.1 g/g from wheat bran, 2.32 g/g from maize hulls, 2.48 g/g from wheat hulls and 4.9 g/g from soybean fiber (Alfredo, Gabriel, Luis, & David, 2009). The increase in the WHC of M-IDF according to the increase in the hydrogen peroxide process might be mainly attributable to the destruction of lignocellulose biomass structure. AHP treatment enhanced the WHC of IDF by removing starch, protein and hemicelluloses in fiber, and improving the specific surface area of fiber and exposing more hydrophilic groups. Besides, in contrast to the results for O-IDF, the surface area and wrinkling in M-IDF increased after AHP treatment. M-IDF with finer particles and a larger surface area, as observed through SEM, had a greater ability to trap water and might have resulted in the increase in WHC, through surface tension strength and/or hydrogen bonds and dipole interactions (Ullah et al., 2018). AHP breaks the intermolecular hydrogen bonds of cellulose and hemicelluloses, thereby improving the exposure of hydrated hydroxide and carboxyl groups and the capillary action of fiber, thus in turn increasing the WHC (Ullah et al., 2018).

The WRC was determined as the ability of a material to retain water, such as linked, hydrodynamic and physically trapped water, under centrifugation conditions (Alfredo et al., 2009). The initial WRC of O-IDF was 4.97 g/g, which was higher than the 3.68 g/g for malt bagasse, 2.13 g/g for oat hulls, and 2.58 g/g for rice hulls, maize hulls (3.17 g/g), wheat hulls (2.91 g/g) and soybean fiber (1.42 g/g) (Jacometti et al., 2015) (Alfredo et al., 2009). The WRC of the treated samples (M-IDF) exhibited a significant ($p < 0.05$) increase to 7.16 g/g. The increase in WRC caused by AHP treatment might have occurred because of a much looser structure; the exposure of polar groups and other water-binding sites thus may have increased water extra- and inter-linking within IDF.

The measurement steps and principles for ORC were fundamentally the same as those for WRC. The ORC of plant material depends on the surface characteristics, total charge density and hydrophobicity of fiber particles (Zheng & Li, 2018). At present, many consumers restrict the amount of ingested fat and calories in their diet, through intake of low-fat products using DF as a fat replacement, such as meat products (Namir, Siliha, & Ramadan, 2015). Consequently, the ability of DF to retain oil, which is related to some functional properties such as the capacity to decrease serum cholesterol levels and remove excess fat from the human body, is very important for food applications (Chen et al., 2015). Fig. 3(a) depicts the effect of AHP on the ORC of buckwheat straw IDF. Similarly to its effects on water-holding capacity, the AHP treatment significantly increased the ORC of O-IDF from 3.26 g/g to 5.36 g/g, a value higher than the 2 g/g for barley fiber and the 2.3 g/g for jack bean fiber, and lower than the 3.63 g/g for wheat IDF ($p < 0.05$) and the 6.93 g/g for pea fiber (Alfredo et al., 2009). Generally, the AHP increased the adsorption sites of IDF, thereby probably contributing to a substantial improvement in the oil-holding capacity. As shown by SEM, M-IDF had a looser texture than O-IDF after AHP treatment. The appearance of lamellar structure and increased wrinkling and exposure of the fiber surface area, as well as capillary attraction, consequently enhanced the physical entrapment of oil. The water swelling capacity was defined as the volume changes of a certain weight of dry fiber after equilibrium in excess solvent and is associated with many factors such as solvent nature and network density (Zhang et al., 2017). The WSC of IDF was strongly related to the characteristics of the major components and the physical structure of the fiber matrix (Raghavendra et al., 2006). According to Fig. 3(a), M-IDF had a WSC of 14.3 g/g after AHP treatment, followed by a 4.4 g/g WRC of O-IDF. The WSC value of M-IDF significantly ($p < 0.01$) increased by three fold, a value higher than the 4.53 g/g for malt bagasse, the 3.56 g/g for oat hulls and the 3.27 g/g for rice hulls and buckwheat bran IDF powder, with 5.31 mL water/g fiber (Jacometti et al., 2015; Wen et al., 2017). The increased WSC after hydrogen peroxide treatment might have resulted from the degradation of cellulose lignin by AHP. Research had demonstrated that AHP can break the linkages of cellulose and

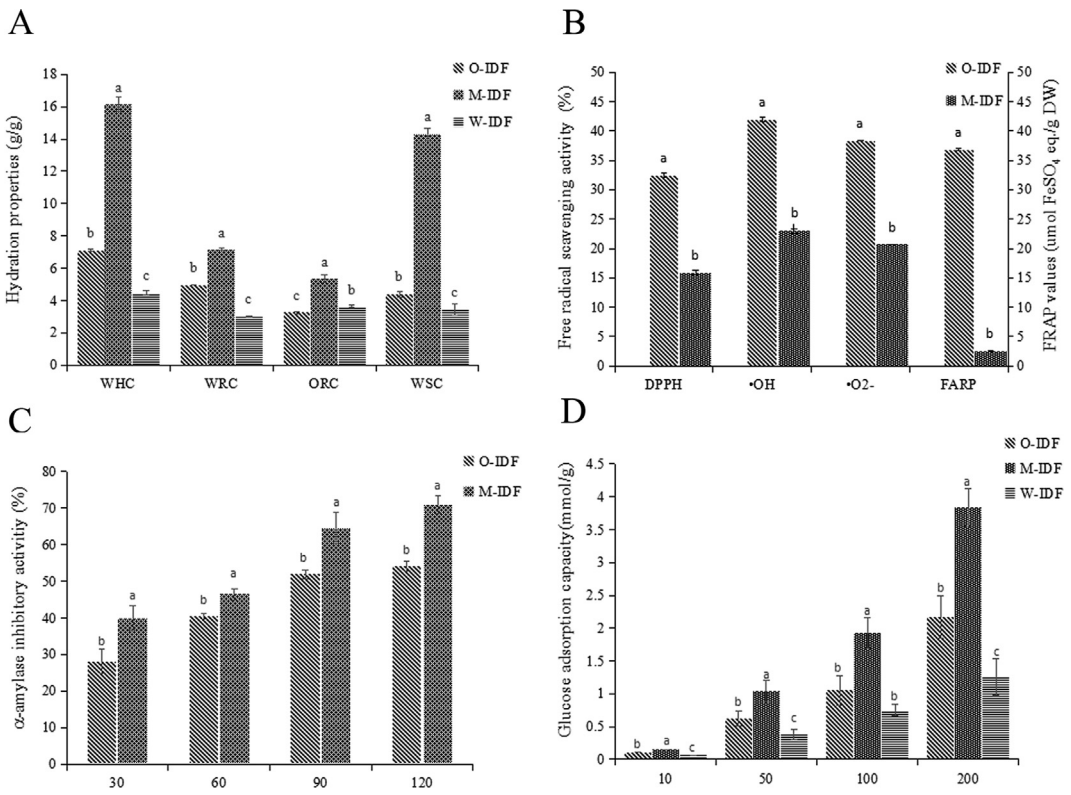

Fig. 3. Hydration properties (A), Evaluation of antioxidant capacity (B), α -amylase inhibitory activity (C), Glucose adsorption capacity (D) before and after modification. WHC, water holding capacity; WRC, water retention capacity; ORC, oil retention capacity; WSC, water swelling capacity; DPPH, DPPH radical scavenging capacity; FARP, ferric ion reducing antioxidant power; ·OH, hydrogen peroxide; $\cdot O^{2-}$, superoxide peroxide; O-IDF, original buckwheat straw insoluble dietary fiber; M-IDF, modified buckwheat straw insoluble dietary fiber treated with alkaline hydrogen peroxide. Bars with different letters above are significantly different from each other ($p < 0.05$).

hemicelluloses, thus leading to destruction of the DF matrix structure. Moreover, degradation of cellulose by AHP treatment breaks the long cellulose chains of DF into short cellulose chains, which can generate space-enlarging effects (Jie & Shaoying, 2005). The disintegrated structure exposes more hydrogen bonds and dipole forms, and also contributes to the high WSC. In general, the effect of the AHP on the hydration and adsorption properties of IDF is determined not only by the particle size of the fiber but also by the composition, molecular structure, surface area, fibrous matrix properties and porosity of the DF (Zhao et al., 2018). AHP treatment has been reported to break the covalent bonds between cellulose and hemicelluloses, and the ether bonds between hemicelluloses and lignin, thus disintegrating the physical structure of IDF. The looser structure, larger surface area and more exposed polar groups contributed to the improvement in the hydration and adsorption properties of IDF. These results demonstrated the potential for use of AHP treatment in preparing DF ingredients for functional foods.

3.7. Evaluation of antioxidant capacity

The antioxidant activity of plant materials is a major topic of global interest and has been the subject of a wide range of research in recent years (Nieto Calvache et al., 2016). The antioxidant capacity of IDF was evaluated through two methods: one was based on radical scavenging capacity, and the other was based on the metal reducing power of a sample (Sanz-Pintos et al., 2017). Fig. 3(b) summarizes the results of antioxidant power. As a common antioxidant assay, scavenging of DPPH is a method used to determine the ability of plant materials to provide hydrogen atoms and scavenge lipophilic free radicals. Compared with that of O-IDF, the DPPH scavenging ability of M-IDF decreased to 15.80% after hydrogen peroxide treatment. As indicated in Fig. 3(a), the scavenging ability of hydroxyl radicals and superoxide anions also decreased after AHP treatment. Notably, the hydroxyl radical scavenging capacity and superoxide anion scavenging capacity of IDF after AHP treatment not only showed the same trend but also had a similar degree of reduction. The 50% decrease in the scavenging ability of hydroxyl radicals and superoxide anions of M-IDF was evident as compared with that of O-IDF. The possible reasons for this phenomenon are as follows. In AHP treatment, hydrogen peroxide anions could react with H_2O_2 to form hydrogen peroxide and hydroxyl radical in the alkaline medium $H_2O_2 + HOO^- \rightarrow OH\cdot + O_2^-\cdot + H_2O$. Then in the absence of other reagents, superoxide and hydroxyl radicals could combine to generate oxygen and water $OH\cdot + O_2^-\cdot + H^+ \rightarrow O_2 + H_2O$ (Dutra et al., 2018; Lewis et al., 1988). In this series of reactions, the hydroxyl and superoxide anion radicals remain in a molar ratio of 1:1. The molar mass of free radicals produced in the reaction solution is equal, thus leading to a decrease by the same degree of the radical scavenging capacity of IDF. The FRAP method, also called the determination of total reductive power, is a method used to determine the metal reducing power in aqueous solutions. Antioxidant compounds cause the reduction of the ferric (Fe^{3+}) form to the ferrous (Fe^{2+}) form, because of their reductive capability (Cheng et al., 2017). Ferrous ions form a blue complex with 2,4,6-tripyridin-2-yl-1,3,5-triazine (TPTZ). The higher ferrous ion equivalent ($FeSO_4$ eq./g DW) is an indication of a material's higher antioxidant capacity. This principle was utilized to study the antioxidant potential of IDF. As shown in Fig. 3(a), the antioxidant capacity of O-IDF, as evaluated by FRAP assays, was 56 μmol FeSO4 eq./g DW, whereas that of M-IDF was 15 μmol FeSO4 eq./g DW. The reducing power of M-IDF showed a nearly four-fold lower absorbance than that of O-IDF. After AHP treatment, the FARP value decreased to a greater extent as compared with that of other methods, possibly because of the differences in reaction substrate. The FARP

assay indicated the total antioxidant capacity of the sample, whereas the DPPH method and scavenging capacity of hydroxyl radicals and superoxide anions focused on certain types of free radical. In general, the antioxidant capacity of IDF showed a downward trend in Fig. 3(a). Several other reports have described similar phenomena (Lewis et al., 1988). On the one hand, Dutra et al. (2018) reported that AHP treatment destroys the structure of lignocellulose biomass. On account of changing or damaging the fiber matrix, AHP causes some phenolics that are linked or embedded in the matrix to be released or exposed. The change in phenolic compounds in IDF after AHP treatment is shown in Table 3. In addition, along with the depolymerization of fiber lignin caused by AHP, the antioxidant abilities of IDF decreased, results consistent with the change in phenolic content H_2O_2, a strong oxidizer, could have provided electrons. Substances in IDF trapped the electrons provided by hydrogen peroxide, thereby decreasing the antioxidant capacity. Thus, a correlation was observed between antioxidation and polyphenol content.

3.8. α-amylase inhibitory activity

The enzyme α-amylase is a major factor involved in the release of glucose from starch in the intestine. When amylase is suppressed, the content of small molecule sugars hydrolyzed from starch is limited to control blood sugar levels (Cheng et al., 2017). Similarly to inhibition of α -glucosidase, inhibition of amylase is another strategy for managing type 2 diabetes (Im & Yoon, 2015). The α-amylase inhibitors derived from natural plant materials are an attractive strategy for controlling postprandial blood glucose. The inhibitory effect of IDF is related to microstructure, particle size, WSC and the structure of crystalline cellulose; it is an important factor in evaluating the ability of DF to retard glucose production as a functional food component in vitro (Zheng & Li, 2018).

As shown in Fig. 3(c), the α-amylase inhibitory activity of O-IDF and M-IDF was elevated with increased hydrolysis time. The α -amylase inhibitory activities of O-IDF presented an upward trend over time, displaying a positive correlation. For example, the inhibitory activity of O-IDF and M-IDF increased from 28.10 and 40.00% (enzymolysis at 30 min) to 54.08 and 70.94% (2 h of hydrolysis), respectively, at a concentration of 100 mg. When immersed in the starch mixture, IDF expanded gradually by absorbing water over time. With the gradual exposure of the internal structure and polar groups of IDF and the improvement in the physical barrier, the inhibition ability of amylase increased. This observation may provide a possible explanation for the relationship between enzyme hydrolysis time and the inhibition rate of amylase in IDF. Moreover, O-IDF also showed 70.9% α -amylase inhibitory activity at an enzymolysis time of 120 min, followed by 90 min (64.6%) and 60 min (46.4%), values higher than the 6.33%–24.72% in rice bran fiber, 10.52%–14.51% in coconut cake DF and 28.82–31.03% in coconut cake DF hydrolyzed by cellulases as well as the 10.56% in soybean (Qi et al., 2015; Zheng & Li, 2018). Notably, the α -amylase inhibition rate of O-IDF at 120 min was not significantly different from that at 90 min. This result was probably caused by full swelling and the maximum barrier effect in IDF. M-IDF exhibited higher α -amylase inhibitory activities than O-IDF at any time of enzymatic hydrolysis, perhaps because of the looser structure (Fig. 2) and the higher WHC, WRC and WSC (Fig. 3(a)), thus representing the ability to decrease the contact rate between α-amylase and starch. The O-IDF, untreated by AHP, comprised a complete lignocellulosic biomass. Although it was considered to be an antioxidant that hinders the digestion of nutrients in the intestines, the physical structure was tight, thus leading to poor palatability. The links among cellulose and hemicelluloses, hemicelluloses and lignin might break during AHP treatment, thereby leading to disintegration of lignocellulosic biomass (Doner, Sweeney, & Hicks, 2000; Dutra et al., 2018; Gellerstedt, Hardell, & Lindfors, 1980). M-IDF with a larger surface area and lamellar structure maximizes starch sorption and the barrier of amylase combining to starch, thus delaying the release of glucose. Im and Yoon (2015) have found that fiber can decrease levels of postprandial serum glucose by hindering glucose diffusion, decreasing the glucose concentration in the small intestine, delaying the decomposition of starch and directly inhibiting enzymes. The results from our investigation indicated that M-IDF might decrease the rate of glucose absorption as well as the concentration of postprandial serum glucose through inhibiting the effect of α -amylase.

3.9. Glucose adsorption capacity

A series of different concentrations of glucose were used to investigate the glucose adsorption capacity of DF. In the experiments, glucose dissolved in solution was absorbed by IDF in vitro. This value was used to demonstrate the behavior of fiber in adsorbing glucose during the gastrointestinal transit time (Peerajit, Chiewchan, & Devahastin, 2012). In Fig. 3(d), variations of adsorbed glucose after the addition of O-IDF and M-IDF or commercial wheat DF preparations for comparison are presented. With the incremental glucose concentrations (10–200 μmol/g), the glucose adsorbed by O-IDF and M-IDF was 0.1–2.17 mmol/g and 0.15–3.84 mmol/g, respectively, values significantly ($p < 0.05$) greater than those (0.06–1.26 mmol/g) of the wheat IDF control. The possible explanation for these results was that, unlike wheat, buckwheat, known as a pseudo grain, belongs to Fagopyrum Mill, Polygonaceae. The main reason for the high resistance in the unique growth environment might be the different proportions and compositions of cellulose, hemicelluloses and lignin in buckwheat straw, which have different functional properties. Moreover, all IDF samples were able to effectively combine glucose at different glucose concentrations (10–200 mmol/L), and the glucose content in combination with DF was concentration-dependent, findings consistent with the results of a previous study (Liu, Wang, Liu, & Pan, 2016). In Fig. 3(d) M-IDF had the greatest glucose adsorption capacity, with 3.84 mmol/g in 200 mmol/L glucose concentrations, followed by O-IDF (2.17 mmol/g); values that were higher than those of commercial wheat IDF (1.26 mmol/g), rice bran fiber (0.01–1.04 mmol/g) (Xie et al., 2017), resistant starch and insoluble fibers derived from wheat bran (0.05–0.56 mmol/g at 5–100 mmol/L glucose) (Ou, Kwok, Li, & Fu, 2001), sweet potato DF (0.54–1.27 mmol/g) and wheat bran DF (0.45–0.56 mmol/g) (Chen et al., 2015), but lower than those of insoluble fractions prepared from citrus peels (3.68–5.14–18.5–23.3 mmol/g at 10–200 mmol/L glucose) (Peerajit et al., 2012).

The AHP treatment had a strong effect on the GAC of IDF. Compared with O-IDF, the M-IDF exhibited better glucose adsorption at any concentration of glucose. IDF effectively absorbs glucose and retards glucose diffusion through chemisorption, physical barriers and entrapment of glucose molecules (Chau, Huang, & Lee, 2003). According to SEM and XRD analysis, AHP treatment can break the strong links in lignocellulosic biomass, thus resulting in more polar groups and a more open internal structure in M-IDF. This treatment therefore might enhance the chemical adsorption of glucose molecules by IDF. In addition, the physical obstacles of M-IDF particles, such as the greater available surface and fissures, might decrease the exposure of glucose molecules to the wall of the small intestine. The IDF would therefore trap glucose molecules and embed them in the fiber network, thus diminishing glucose content in the supernatant.

Both O-IDF and M-IDF exhibited a potential to control postprandial blood glucose in the body. The enhancement in glucose adsorbing ability of M-IDF markedly improved the intestinal function. The properties of M-IDF also make it suitable as a low-calorie ingredient for fiber enrichment and dietetic snacks.

4. Conclusion

Results of this study revealed that buckwheat straw is an ideal material for IDF recovery, and AHP treatment effectively improved the

functional characteristics of IDF by breaking the covalent links among cellulose, hemicelluloses and lignin. The hydrolysis of hemicelluloses and the amorphous portion in cellulose effectively altered the monosaccharide composition of IDF, especially the percentages of glucose and xylose. In addition, the increase in the cellulose ratio led to an improvement in crystallinity. Compared with O-IDF, M-IDF had a lower content of polyphenols, chroma and antioxidant activity, because of the removal and destruction of lignin and polyphenol. However, M-IDF exhibited enhanced physiological properties such as WHC, WRC, ORC, WSC, GAC and α -amylase inhibitory activity inhibition, owing to a loosening of the IDF structure and exposure of internal groups. Our results suggest that AHP treatment effectively improves the functionality of IDF, a potential fiber-rich ingredient in functional foods.

Declaration of Competing Interest

None.

Acknowledgements

This work was supported by National Industrial Construction Project of Modern Agriculture Technology (oats & buckwheat) (grant numbers CARS-08-D2) and Science & Industry Coordination Project of Innovation (grant numbers 2017CXY-13). Both of them belong to China.

Appendix A. Supplementary data

Supplementary data to this article can be found online at https://doi.org/10.1016/j.fochx.2019.100029.

References

Alfredo, V. O., Gabriel, R. R., Luis, C. G., & David, B. A. (2009). Physicochemical properties of a fibrous fraction from chia (Salvia hispanica L.). *LWT - Food Science and Technology, 42*(1), 168–173. https://doi.org/10.1016/j.lwt.2008.05.012.

Carlos, A. A. V. (2016). An aggregated understanding of alkaline hydrogen peroxide (ahp) pretreatment of biomass and hemicellulose conversion. (Doctoral dissertation).

Chau, C. F., Huang, Y. L., & Lee, M. H. (2003). In vitro hypoglycemic effects of different insoluble fiber-rich fractions prepared from the peel of citrus Sinensis L. cv Liucheng. *Journal of Agricultural and Food Chemistry, 51*(22), 6623–6626. https://doi.org/10.1021/jf034449y.

Chen, J., Zhao, Q., Wang, L., Zha, S., Zhang, L., & Zhao, B. (2015). Physicochemical and functional properties of dietary fiber from maca (Lepidium meyenii Walp.) liquor residue. *Carbohydrate Polymers, 132*, 509–512. https://doi.org/10.1016/j.carbpol.2015.06.079.

Cheng, L., Zhang, X., Hong, Y., Li, Z., Li, C., & Gu, Z. (2017). Characterisation of physicochemical and functional properties of soluble dietary fibre from potato pulp obtained by enzyme-assisted extraction. *International Journal of Biological Macromolecules, 101*, 1004–1011. https://doi.org/10.1016/j.ijbiomac.2017.03.156.

Diedericks, C. F., & Jideani, V. A. (2015). Physicochemical and Functional Properties of Insoluble Dietary Fiber Isolated from Bambara Groundnut (*Vigna subterranea* [L.] Verdc.). *Journal of Food Science, 80*(9), C1933–C1944. https://doi.org/10.1111/1750-3841.12981.

Doner, L. W., Sweeney, G. A., & Hicks, K. B. (2000). Isolation of hemicellulose from corn fiber. https://doi.org/10.1094/CCHEM.1997.74.2.176.

Dutra, E. D., Santos, F. A., Alencar, B. R. A., Reis, A. L. S., de Souza, R. de F. R., Aquino, K. A., ... Menezes, R. S. C. (2018). Alkaline hydrogen peroxide pretreatment of lignocellulosic biomass: status and perspectives. *Biomass Conversion and Biorefinery, 8*(1), 225–234. https://doi.org/10.1007/s13399-017-0277-3.

Gellerstedt, G., Hardell, H. L., & Lindfors, E. L. (1980). The reactions of lignin with alkaline hydrogen peroxide. Part IV. Products from the oxidation of quinone model compounds. *Acta Chemica Scandinavica, Series B: Organic Chemistry and Biochemistry*. https://doi.org/10.3891/acta.chem.scand.34b-0669.

Im, H. J., & Yoon, K. Y. (2015). Production and characterisation of alcohol-insoluble dietary fibre as a potential source for functional carbohydrates produced by enzymatic depolymerisation of buckwheat hulls. *Czech Journal of Food Sciences, 33*(5), 449–457. https://doi.org/10.17221/200/2015-CJFS.

Jacometti, G. A., Mello, L. R. P. F., Nascimento, P. H. A., Sueiro, A. C., Yamashita, F., & Mali, S. (2015). The physicochemical properties of fibrous residues from the agro industry. *LWT - Food Science and Technology, 62*(1), 138–143. https://doi.org/10.1016/j.lwt.2015.01.044.

Jie, H., Shaoying, Z. (2005). Effect of ultra - fine pulverization by wet processing on particle structure and physical properties of soybean dietary fiber, 10, 90–94.

Kalinová, J. P., Vrchotová, N., & Tříska, J. (2018). Contribution to the study of rutin stability in the achenes of Tartary buckwheat (Fagopyrum tataricum). *Food Chemistry, 258*(March), 314–320. https://doi.org/10.1016/j.foodchem.2018.03.090.

Lewis, S. M., Montgomery, L., Garleb, K. A., Berger, L. L., & Fahey, G. C. (1988). Effects of alkaline hydrogen peroxide treatment on in vitro degradation of cellulosic substrates by mixed ruminal microorganisms and Bacteroides succinogenes S85. *Applied and Environmental Microbiology, 54*(5), 1163–1169.

Li, N., Feng, Z., Niu, Y., & Yu, L. L. (2018). Structural, rheological and functional properties of modified soluble dietary fiber from tomato peels. *Food Hydrocolloids, 77*, 557–565. https://doi.org/10.1016/j.foodhyd.2017.10.034.

Liu, Y., Wang, L., Liu, F., & Pan, S. (2016). Effect of grinding methods on structural, physicochemical, and functional properties of insoluble dietary fiber from orange peel. *International Journal of Polymer Science, 2016*. https://doi.org/10.1155/2016/6269302.

Ma, M., & Mu, T. (2016). Modification of deoiled cumin dietary fiber with laccase and cellulase under high hydrostatic pressure. *Carbohydrate Polymers, 136*, 87–94. https://doi.org/10.1016/j.carbpol.2015.09.030.

Namir, M., Siliha, H., & Ramadan, M. F. (2015). Fiber pectin from tomato pomace: characteristics, functional properties and application in low-fat beef burger. *Journal of Food Measurement and Characterization, 9*(3), 305–312. https://doi.org/10.1007/s11694-015-9236-5.

Nieto Calvache, J., Cueto, M., Farroni, A., de Escalada Pla, M., & Gerschenson, L. N. (2016). Antioxidant characterization of new dietary fiber concentrates from papaya pulp and peel (Carica papaya L.). *Journal of Functional Foods, 27*, 319–328. https://doi.org/10.1016/j.jff.2016.09.012.

Ou, S., Kwok, K., Li, Y., & Fu, L. (2001). In vitro study of possible role of dietary fiber in lowering postprandial serum glucose. *Journal of Agricultural and Food Chemistry, 49*(2), 1026–1029. https://doi.org/10.1021/jf000574n.

Peerajit, P., Chiewchan, N., & Devahastin, S. (2012). Effects of pretreatment methods on health-related functional properties of high dietary fibre powder from lime residues. *Food Chemistry, 132*(4), 1891–1898. https://doi.org/10.1016/j.foodchem.2011.12.022.

Qi, J., Li, Y., Yokoyama, W., Majeed, H., Masamba, K. G., Zhong, F., & Ma, J. (2015). Cellulosic fraction of rice bran fibre alters the conformation and inhibits the activity of porcine pancreatic lipase. *Journal of Functional Foods, 19*, 39–48. https://doi.org/10.1016/j.jff.2015.09.012.

Raghavendra, S. N., Ramachandra Swamy, S. R., Rastogi, N. K., Raghavarao, K. S. M. S., Kumar, S., & Tharanathan, R. N. (2006). Grinding characteristics and hydration properties of coconut residue: A source of dietary fiber. *Journal of Food Engineering, 72*(3), 281–286. https://doi.org/10.1016/j.jfoodeng.2004.12.008.

Rehman, N., de Miranda, M. I. G., Rosa, S. M. L., Pimentel, D. M., Nachtigall, S. M. B., & Bica, C. I. D. (2014). Cellulose and nanocellulose from maize straw: an insight on the crystal properties. *Journal of Polymers and the Environment, 22*(2), 252–259. https://doi.org/10.1007/s10924-013-0624-9.

Sangnark, A., & Noomhorm, A. (2004). Chemical, physical and baking properties of dietary fiber prepared from rice straw. *Food Research International, 37*(1), 66–74. https://doi.org/10.1016/j.foodres.2003.09.007.

Sanz-Pintos, N., Pérez-Jiménez, J., Buschmann, A. H., Vergara-Salinas, J. R., Pérez-Correa, J. R., & Saura-Calixto, F. (2017). Macromolecular antioxidants and dietary fiber in edible seaweeds. *Journal of Food Science, 82*(2), 289–295. https://doi.org/10.1111/1750-3841.13592.

Sheltami, R. M., Abdullah, I., Ahmad, I., Dufresne, A., & Kargarzadeh, H. (2012). Extraction of cellulose nanocrystals from mengkuang leaves (Pandanus tectorius). *Carbohydrate Polymers, 88*(2), 772–779. https://doi.org/10.1016/j.carbpol.2012.01.062.

Ullah, I., Yin, T., Xiong, S., Huang, Q., Zia-ud-Din, Zhang, J., & Javaid, A. B. (2018). Effects of thermal pre-treatment on physicochemical properties of nano-sized okara (soybean residue) insoluble dietary fiber prepared by wet media milling. *Journal of Food Engineering, 237*(April), 18–26. https://doi.org/10.1016/j.jfoodeng.2018.05.017.

Vitaglione, P., Napolitano, A., & Fogliano, V. (2008). Cereal dietary fibre: a natural functional ingredient to deliver phenolic compounds into the gut. *Trends in Food Science and Technology, 19*(9), 451–463. https://doi.org/10.1016/j.tifs.2008.02.005.

Wang, X., Zhang, L., Wu, J., Xu, W., Wang, X., & Lü, X. (2017). Improvement of simultaneous determination of neutral monosaccharides and uronic acids by gas chromatography. *Food Chemistry, 220*, 198–207. https://doi.org/10.1016/j.foodchem.2016.10.008.

Webber, V., Dutra, S. V., Spinelli, F. R., Marcon, Â. R., Carnieli, G. J., & Vanderlinde, R. (2014). Effect of glutathione addition in sparkling wine. *Food Chemistry, 159*, 391–398. https://doi.org/10.1016/j.foodchem.2014.03.031.

Wen, Y., Niu, M., Zhang, B., Zhao, S., & Xiong, S. (2017). Structural characteristics and functional properties of rice bran dietary fiber modified by enzymatic and enzyme-micronization treatments. *LWT - Food Science and Technology, 75*, 344–351. https://doi.org/10.1016/j.lwt.2016.09.012.

Xie, F., Wang, Y., Wu, J., & Wang, Z. (2017). Insoluble dietary fibers from Angelica keiskei by-product and their functional and morphological properties. *Starch/Staerke, 69*(3–4), 1–12. https://doi.org/10.1002/star.201600122.

Yan, X., Ye, R., & Chen, Y. (2015). Blasting extrusion processing: The increase of soluble dietary fiber content and extraction of soluble-fiber polysaccharides from wheat bran. *Food Chemistry, 180*, 106–115. https://doi.org/10.1016/j.foodchem.2015.01.127.

Yu, G., Bei, J., Zhao, J., Li, Q., & Cheng, C. (2018). Modification of carrot (Daucus carota Linn. var. Sativa Hoffm.) pomace insoluble dietary fiber with complex enzyme method, ultrafine comminution, and high hydrostatic pressure. *Food Chemistry, 257*(17), 333–340. https://doi.org/10.1016/j.foodchem.2018.03.037.

Yu, D., Chen, J., Ma, J., Sun, H., Yuan, Y., Ju, Q., ... Luan, G. (2018). Effects of different milling methods on physicochemical properties of common buckwheat flour. *LWT - Food Science and Technology, 92*(December 2017), 220–226. https://doi.org/10.

1016/j.lwt.2018.02.033.
Zhang, J., Wang, Y. H., Qu, Y. S., Wei, Q. Y., & Li, H. Q. (2018). Effect of the organizational difference of corn stalk on hemicellulose extraction and enzymatic hydrolysis. *Industrial Crops and Products, 112*(July 2017), 698–704. https://doi.org/10.1016/j.indcrop.2018.01.007.
Zhang, W., Zeng, G., Pan, Y., Chen, W., Huang, W., Chen, H., & Li, Y. (2017). Properties of soluble dietary fiber-polysaccharide from papaya peel obtained through alkaline or ultrasound-assisted alkaline extraction. *Carbohydrate Polymers, 172*, 102–112. https://doi.org/10.1016/j.carbpol.2017.05.030.
Zhao, G., Zhang, R., Dong, L., Huang, F., Tang, X., Wei, Z., & Zhang, M. (2018). Particle size of insoluble dietary fiber from rice bran affects its phenolic profile, bioaccessibility and functional properties. *LWT - Food Science and Technology, 87*, 450–456. https://doi.org/10.1016/j.lwt.2017.09.016.
Zheng, Y., & Li, Y. (2018). Physicochemical and functional properties of coconut (Cocos nucifera L) cake dietary fibres: Effects of cellulase hydrolysis, acid treatment and particle size distribution. *Food Chemistry, 257*(November 2017), 135–142. https://doi.org/10.1016/j.foodchem.2018.03.012.
Zhou, X. L., Qian, Y. F., Zhou, Y. M., & Zhang, R. (2011). Effect of enzymatic extraction treatment on physicochemical properties, microstructure and nutrient composition of tartary buckwheat bran: A new source of antioxidant dietary fiber. *Advanced Materials Research, 396–398*, 2052–2059. https://doi.org/10.4028/www.scientific.net/AMR.396-398.2052.